SUPPLEMENTAL MATERIAL 2

to

Low-temperature gas-phase oxidation of diethyl ether: fuel reactivity and fuel-specific products

Luc-Sy Tran[1,2,3,*], Olivier Herbinet[2], Yuyang Li[4], Julia Wullenkord[1], Meirong Zeng[4], Eike Bräuer[1], Fei Qi[4], Katharina Kohse-Höinghaus[1], Frédérique Battin-Leclerc[2]

[1] *Department of Chemistry, Bielefeld University, Universitätsstraße 25, D-33615 Bielefeld, Germany*

[2] *Laboratoire Réactions et Génie des Procédés (LRGP), CNRS, Université de Lorraine, ENSIC, 1, rue Grandville, BP 20451, 54001 Nancy Cedex, France*

[3] *Université de Lille, CNRS, UMR 8522 - PC2A - Physicochimie des Processus de Combustion et de l'Atmosphère, F-59000 Lille, France*

[4] *School of Mechanical Engineering, Shanghai Jiao Tong University (SJTU), Shanghai 200240, PR China*

* Corresponding author: Dr. Luc-Sy Tran
Université de Lille, CNRS, UMR 8522 - PC2A - Physicochimie des Processus de Combustion et de l'Atmosphère, F-59000 Lille, France.
E-mail: luc-sy.tran@univ-lille1.fr

Proc. Combust. Inst. 37, 2019

Table of contents:

S.I. Additional information about the present kinetic model

While the main features of the proposed DEE LT sub-mechanism are described in the main paper, a list of the considered reaction classes and the used kinetic data are detailed here.

List of the considered reaction classes:

(1) R + O_2 <=> ROO (first O_2 addition; R: fuel radicals; ROO: ethoxyethylperoxy radicals)

(2) R + ROO <=> RO + RO

(3) R + HO_2 <=> RO + OH

(4) R + $C_XH_YO_2$ <=> RO + C_XH_YO (C_XH_Y: CH_3, C_2H_5)

(5) ROO + ROO <=> RO + RO + O_2

(6) ROO + ROO <=> ester/aldehyde + alcohol + O_2 (recombination/disproportionation)

(7) ROO + $C_XH_YO_2$ <=> RO + C_XH_YO + O_2

(8) ROO + $C_XH_YO_2$ <=> ester/aldehyde + alcohol + O_2

(9) ROO + R" <=> RO + R"O (R": CH_3, C_2H_5, HCO)

(10) ROO + HO_2 <=> ROOH (hydroperoxide) + O_2

(11) ROO + H_2O_2 <=> ROOH + HO_2

(12) ROOH <=> RO + OH

(13) ROO <=> EVE (ethyl vinyl ether) + HO_2 (concerted eliminations)

(14) ROO <=> QOOH (ROO isomerization; QOOH: hydroperoxyl-fuel radicals)

(15) Isomerization between different QOOHs

(16) QOOH <=> ester/aldehyde + OH (QOOH isomerization followed by O–O β-scission)

(17) QOOH <=> cyclic ether + OH (cyclization)

(18) QOOH <=> EVE + HO_2 (radical site beta to OOH group)

(19) C–O or C–C β-scission of QOOH

(20) QOOH + O_2 <=> OOQOOH (second O_2 addition)

(21) OOQOOH <=> HOOQ=O (ketohydroperoxide) + OH

(22) HOOQ=O <=> OQ=O + OH (O–O decomposition of ketohydroperoxide)

(23) HOOQ=O <=> acetic acid + acetic acid (*via* Korcek decomposition)

(24) OQ=O <=> acetic acid + CH_3CO/CH_2CHO

(25) H-abstractions from HOOQ=O followed by O–O β-scission to form acetic anhydride

(26) H-abstractions from OQ=O to form acetic anhydride

(27) OOQOOH <=> HOOPOOH (OOQOOH isomerization)

(28) HOOPOOH decomposition by C–O/C–C β-scission or *via* cyclic-ether-hydroperoxide formation

(29) HOOPOOH + O_2 <=> HOOP(OO)OOH (third O_2 addition)

(30) HOOP(OO)OOH <=> HOOP(OOH)=O (keto-di-hydroperoxide) + OH

(31) Decomposition of HOOP(OOH)=O to small species

The rate coefficients of the addition of O_2 to the fuel radicals (*class 1*, first O_2 addition) forming ethoxyethylperoxy radicals (ROO) were taken from [S1]. The kinetic data of reaction

classes 2-5, 7, 9-12 were estimated based on reactions proposed for LT oxidation of DBE [S2]. Recombination/disproportionation reactions of two ROO radicals or ROO with a $C_XH_YO_2$ radical (*classes 6* and *8*) have been recently demonstrated to be important for LT product formation [S3] and were thus also considered in the present model with rate coefficients based on *classes 5* and *7*, respectively. Kinetic data of *classes 13-19* were taken from calculations of Sakai *et al.* [S4], apart from the reaction $CH_3CHOCH(OOH)CH_3 \rightarrow CH_3CHO+CH_3CHO+OH$ (a reaction in *class 19*) for which averaged rate coefficients between those calculated by Sakai *et al.* [S4] and those proposed empirically by Eble *et al.* [S5] were applied (compare Fig. S1) as discussed in the main text.

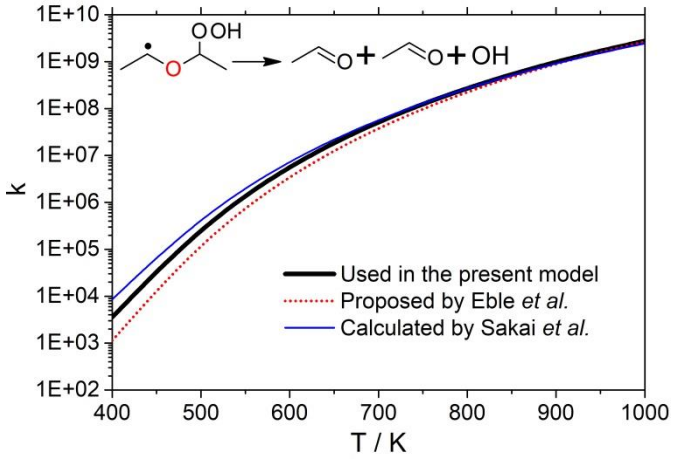

Fig. S1. Rate coefficients of the reaction $CH_3CHOCH(OOH)CH_3 \rightarrow CH_3CHO+CH_3CHO+OH$ (a reaction in *class 19*): comparison of those used in the present model with those proposed by Eble *et al.* [S5] and those calculated by Sakai *et al.* [S4].

Rate coefficients of the second O_2 addition forming OOQOOH (*class 20*) were estimated based on *class 1*. Kinetic data of OOQOOH isomerization followed by a fast O–O β-scission to form ketohydroperoxide (HOOQ=O) (*class 21*) were estimated using the same approach as proposed in Thion *et al.* [S2]. Rate coefficients proposed by these latter authors for the O–O decomposition of ketohydroperoxides were used for reactions of *class 22*. New reaction classes (*classes 23-26*) were also included as discussed in the main paper, with rates coefficients determined based on [S6-S8]. Kinetic data of *classes 27, 28* were estimated based on *classes 14, 17, 19*.

Third O_2 addition reactions (*class 29*) and their subsequent reactions (*classes 30, 31*) were considered with rate coefficients that were estimated based on reaction *classes 20-22*. Furthermore, kinetic data of H-abstractions from DEE by HO_2 were taken from recent calculations by Hu *et al.* [S9], and those by $C_xH_yO_2$ radicals were also included. Rate coefficients of O_2 addition to CH_3CO from the recent measurements of Carr *et al.* [S10] were used. Moreover, subsequent reactions of the formed stable products, such as ethyl acetate, acetic acid, acetic anhydride, 2-methyl-1,3-dioxolane, etc., were either directly taken from recent literature work [S11] or estimated based on structurally-similar species in the core model or from rate rules [S8].

S.II. Examination of the present model against literature HT data

The present model was tested against selected experimental data available in the literature for high temperature (HT) conditions. These include ignition delay times [S12,S13], pyrolysis species profiles [S14], and flame species profiles [S15]. The results are presented in Figs. S2-S4, and show an overall good agreement between the experiment and model.

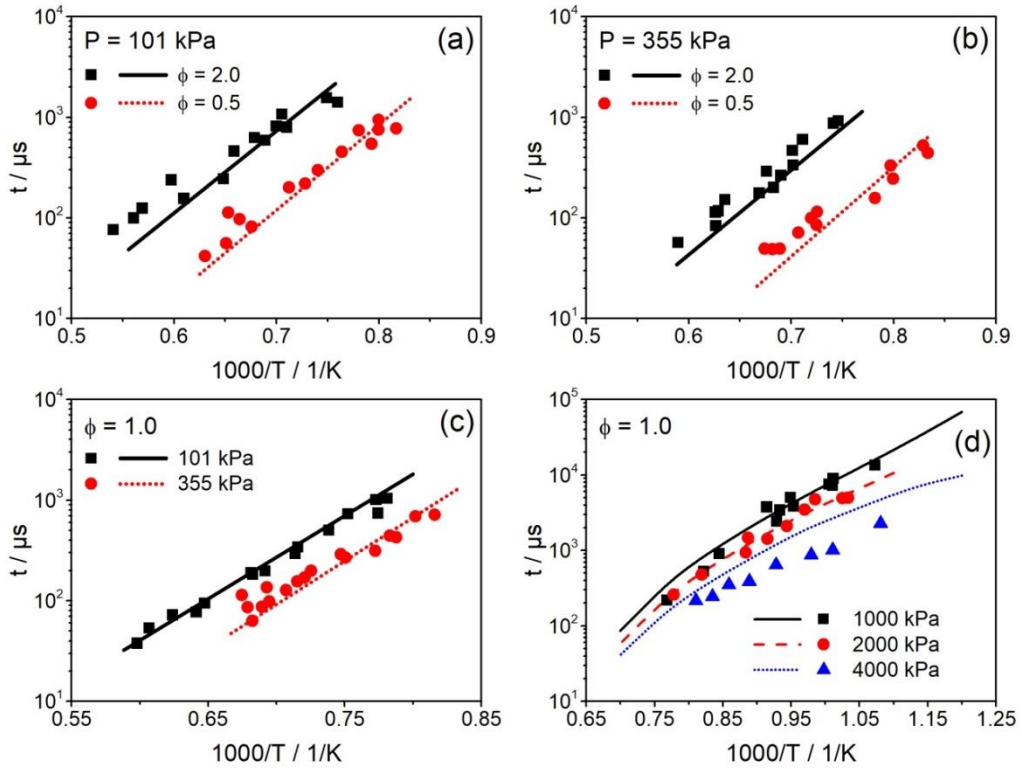

Fig. S2. Examination of the present model (*lines*) against DEE ignition delay time experimental results (*symbols*) of Yasunaga *et al.* [S12] **(a, b,c)** and Werler *et al.* [S13] **(d).**

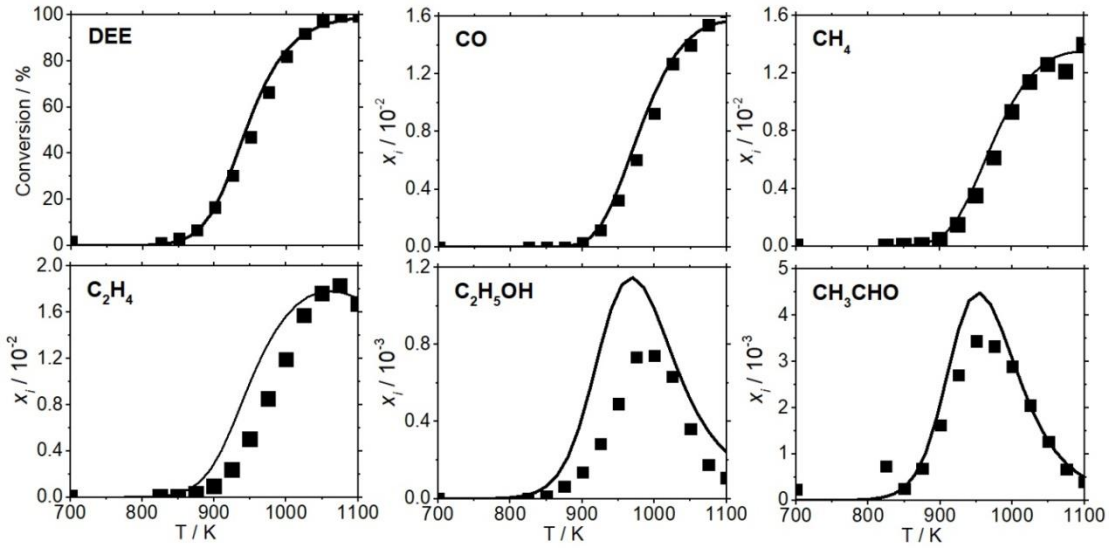

Fig. S3. Examination of the present model (*lines*) against DEE pyrolysis data of Vin *et al.* (2% DEE, 2 s residence time, 106.7 kPa) [S14].

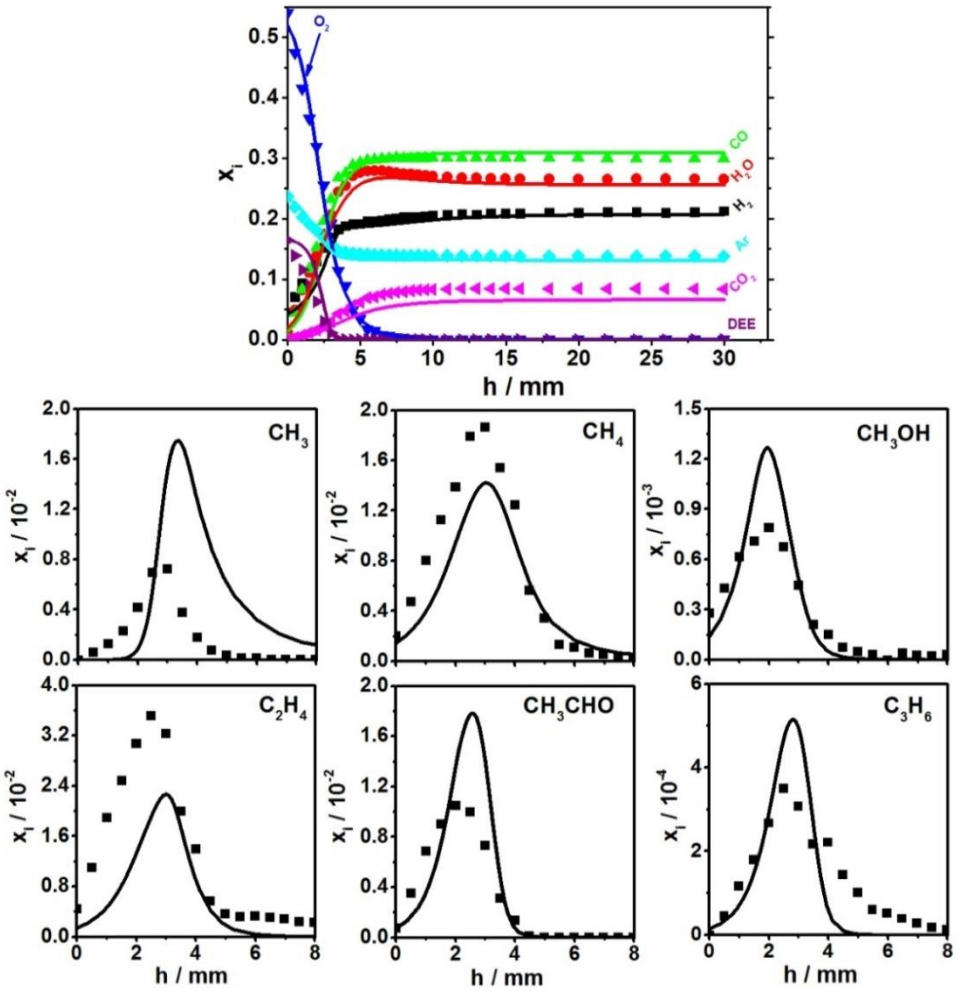

Fig. S4. Examination of the present model (*lines*) against species data of the DEE premixed flame (ϕ=1.8, 4 kPa, 25% Ar) of Tran *et al.* [S15].

S.III. Additional model analyses: sensitivity, OH production rates, comparison to other fuels

Figure S5 presents details of several sensitivity analyses for the DEE consumption under JSR conditions at 560 K (in the first NTC zone) and at 700 K (in the second NTC zone), which were performed using the three models, *i.e.* the present, Eble [S5], and Sakai [S1] models. All three models indicate that H-abstractions from DEE by small oxygenated radicals (OH, HO_2, etc.) strongly promote DEE conversion at both analyzed temperatures, whereas the importance of the first (reaction *r1*) and second (reaction *r3*) O_2 additions, as well as the β-scission of fuel radicals (reaction *r2*) and of the hydroperoxyl-fuel radical (reaction *r4*) changes significantly with temperature. At 560 K, the reaction *r4* inhibits significantly DEE conversion, whereas the reaction *r3* promotes the conversion of this fuel. A competition between these two latter reactions results in the first NTC zone as extensively discussed in the main paper. At 700 K, the reactions *r3* and *r4* disappear from the sensitivity analyses, whereas the reaction *r2* and that of its product ($O_2+C_2H_5=HO_2+C_2H_4$) come into competition with the reaction *r1*, reducing DEE consumption that results in the second NTC zone.

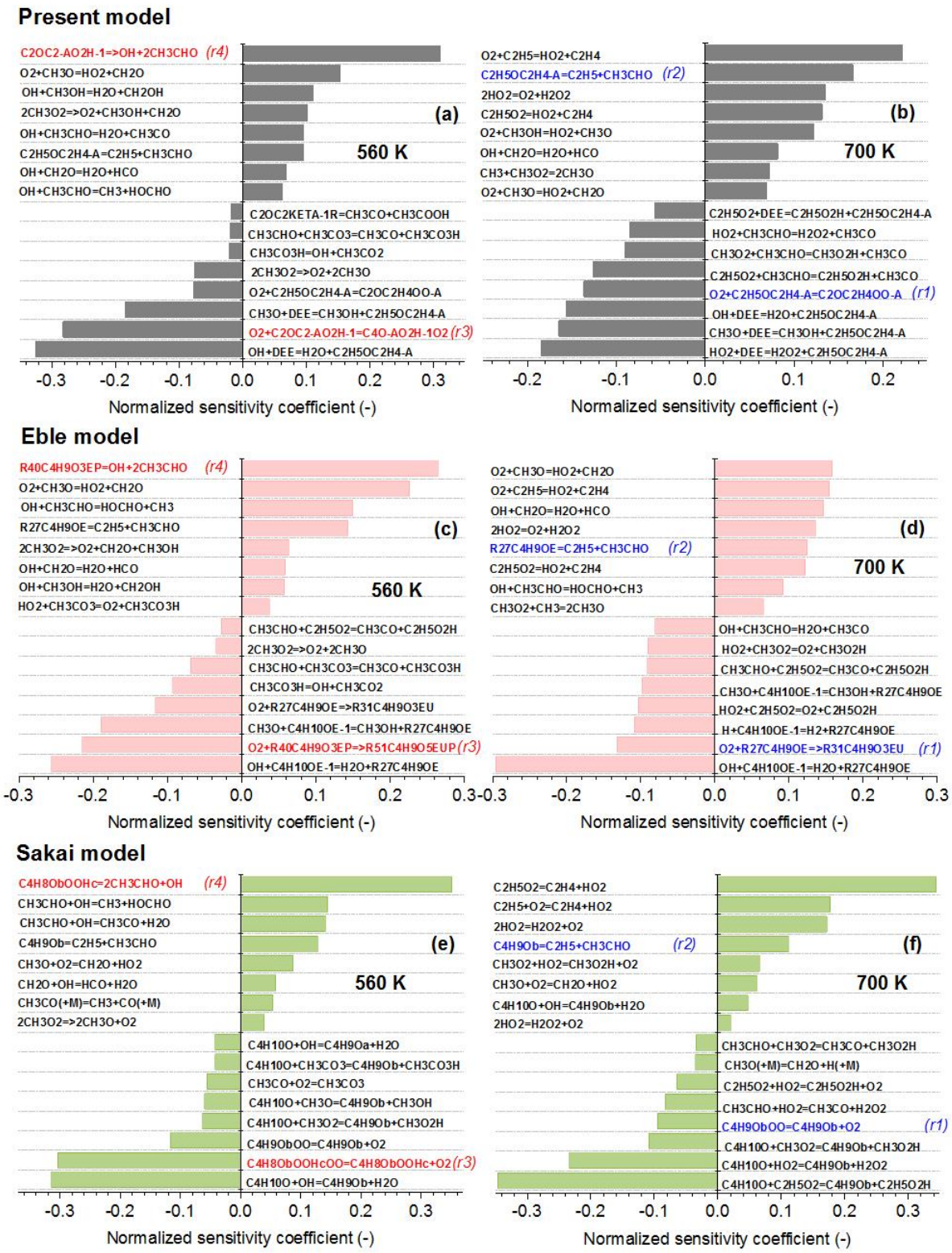

Fig. S5. Sensitivity coefficients for DEE consumption under JSR conditions at 560 K ***(left)*** and 700 K *(right)***.** *Top:* present model, *middle:* Eble model [S5], *bottom:* Sakai model [S1]. Negative coefficients indicate a reaction that increases DEE conversion and vice versa. *r1-r4*: reaction number used in Fig. 2c of the main paper. Chemical nomenclature above corresponds to the assignments in the Chemkin format of the respective models.

Figure S6 presents temperature-dependent OH production rates by different reactions calculated with the present model under the studied JSR conditions. At very low temperature (<525 K), the sum of OH production rates increases due to the formation (C4O-AO2H-1O2=OH+C2OC2KETA-1) as well as the decomposition (C2OC2KETA-1=OH+C2OC2KETA-1R) of a DEE-specific ketohydroperoxide (C2OC2KETA-1), resulting in a quick consumption of DEE. In the range of 525 to 600 K, the OH production decreases, inducing a reduction of DEE conversion. This is the first NTC zone as discussed extensively in the main paper. Above 600 K, OH production rates increase again, resulting mainly from the thermal decomposition of CH_3CO_3H (CH_3CO_3H=OH+CH_3CO_2), and partially from that of CH_3O_2H (CH_3O_2H=OH+CH_3O) and $C_2H_5O_2H$ ($C_2H_5O_2H$=OH+C_2H_5O). In the range of 650-750 K, which is in the second NTC zone, the OH production decreases again. After a transition to HT chemistry above 750 K, OH production raises strongly because of H_2O_2 decomposition and the reaction HO_2+CH_3=OH+CH_3O.

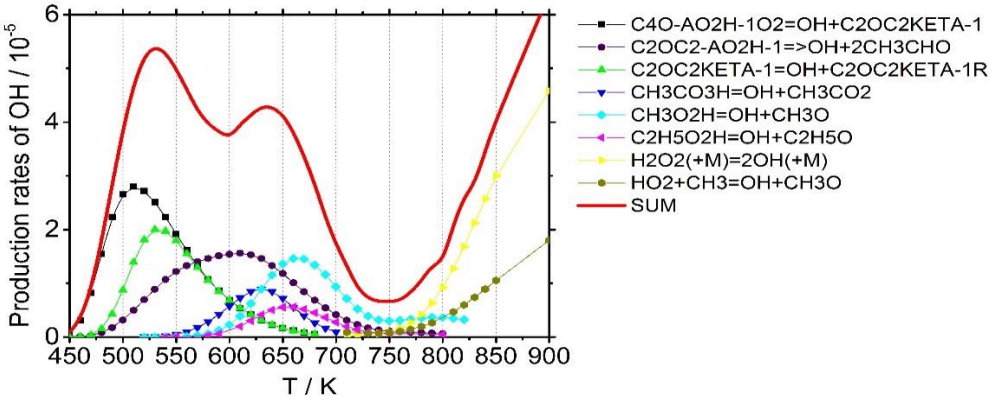

Fig. S6. Temperature-dependent OH production rates (*units: kmol* $m^{-3}s^{-1}$) by different reactions calculated with the present model under the studied JSR conditions. **Sum:** sum of OH production rates by the listed reactions. Chemical nomenclature above corresponds to the assignments in the Chemkin format in the present kinetic mechanism. In the model available in Supplemental Material 1, each species is labeled according to the Simplified Molecular-Input Line-Entry System (SMILES) and with its IUPAC International Chemical Identifier (InChI) to allow for unambiguous identification of the molecular structure.

Figure S7 presents a comparison of the simulated mole fraction profiles of DEE, DME, and *n*-pentane. Simulations were performed at the same conditions using the present model. The sub-models of DME and *n*-pentane developed by the NUI-Galway group [S16,S3] are already contained in the used core model [S3]. While DEE shows two-NTC behavior, this latter behavior has not been observed for *n*-pentane and DME. These two latter fuels only react at higher temperatures (≥550 K).

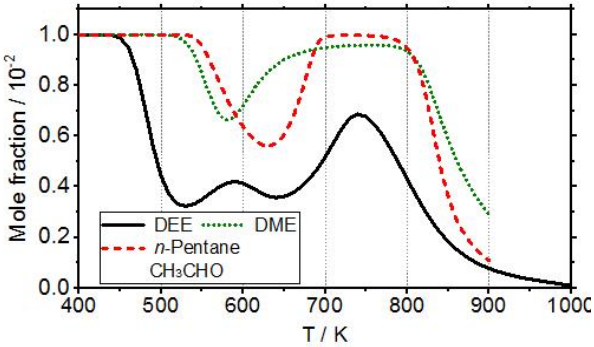

Fig. S7. Comparison of the simulated profile of DEE (using the present model) to those of DME, and *n*-pentane (using the present core model) under the studied JSR conditions.

S.IV. Additional experimental information: carbon balance, main species, table of peak mole fraction of intermediates, PFR intermediate species

Carbon balance

In order to assess the reliability of the obtained experimental results, we checked the carbon atom balance (C-balance) at all studied conditions. The C-balance was calculated from

$$C\text{-}balance\ (\%) = \frac{x_{DEE}^{0} \times n_{C,DEE}}{\sum x_i \times n_{c,i}} \times 100\ ;$$

here x_{DEE}^{0} and $n_{C,DEE}$ represent the initial mole fraction and the carbon number (equal to 4) of DEE, respectively, whereas x_i and $n_{C,i}$ are the mole fraction and the carbon number of the quantified species *i*.

The respective C-balance at selected temperatures in the range of ~400-1100 K is presented in Table S1. The deviation of the C-balance is smaller than 15% in both the PFR and the JSR experiment, indicating good consistency of the obtained experimental results.

Table S1: Carbon balance calculated from quantified species in PFR and JSR. **Deviation:** 100% - *C-balance*.

PFR (x_{DEE}^{0}×4=0.02)			
T / K	$\sum x_i \times n_{c,i}$	**C-balance**	**Deviation**
422	0.0212	105.8%	-5.8%
425	0.0220	109.8%	-9.8%
455	0.0230	115.1%	-15.1%
473	0.0193	96.6%	3.4%
502	0.0180	90.1%	9.9%
527	0.0194	96.8%	3.2%
551	0.0194	97.1%	2.9%
575	0.0189	94.7%	5.3%
603	0.0190	94.8%	5.2%
626	0.0190	95.1%	4.9%
650	0.0198	99.2%	0.8%
677	0.0209	104.3%	-4.3%
700	0.0217	108.7%	-8.7%
728	0.0206	102.9%	-2.9%
773	0.0221	110.3%	-10.3%
801	0.0225	112.7%	-12.7%
823	0.0205	102.4%	-2.4%
851	0.0189	94.7%	5.3%
876	0.0175	87.7%	12.3%
899	0.0175	87.6%	12.4%
917	0.0183	91.3%	8.7%
949	0.0174	87.1%	12.9%
973	0.0174	87.2%	12.8%
1000	0.0183	91.5%	8.5%
1027	0.0188	94.0%	6.0%
1050	0.0183	91.6%	8.4%
1073	0.0181	90.6%	9.4%
1100	0.0197	98.6%	1.4%
1123	0.0206	103.0%	-3.0%

JSR (x_{DEE}^{0}×4=0.04)			
T / K	$\sum x_i \times n_{c,i}$	**C-balance**	**Deviation**
400	0.0401	100.2%	-0.2%
425	0.0399	99.7%	0.3%
450	0.0394	98.4%	1.6%
475	0.0405	101.3%	-1.3%
500	0.0380	95.1%	4.9%
525	0.0360	89.9%	10.1%
550	0.0354	88.6%	11.4%
575	0.0359	89.8%	10.3%
600	0.0380	94.9%	5.1%
625	0.0382	95.6%	4.4%
650	0.0375	93.7%	6.3%
675	0.0374	93.4%	6.6%
700	0.0399	99.8%	0.2%
800	0.0403	100.7%	-0.7%
825	0.0376	94.0%	6.0%
850	0.0385	96.2%	3.8%
900	0.0378	94.5%	5.5%
950	0.0366	91.5%	8.5%
1000	0.0356	89.1%	10.9%
1100	0.0380	95.1%	4.9%

Temperature-dependent mole fraction profiles of major species

Figures S8 and S9 present the mole fraction profiles of major species from JSR (DEE, O_2, CO, CO_2) and PFR (DEE, O_2, CO, CO_2, H_2, H_2O), respectively. While with the used GC-JSR system H_2 and H_2O could not be quantified, these two species were well measured with PFR-EI-MBMS. The two-NTC behavior is evident in the profile shape of fuel and O_2 as well as major products that show two peaks in the two highest LT fuel conversion zones. The present model shows also a two-NTC-zone behavior in both JSR and PFR and reproduce satisfactorily the profiles of major species in several interested temperature windows although some model/experiment discrepancies are noted for CO at very LT in the JSR experiment and for all species in a temperature range of 600-800 K in the PFR experiment. A model analysis at 550 K under JSR conditions indicates that reactions of the core mechanism are responsible for the formation of CO, especially by the reactions $HCO+O_2=CO+HO_2$ and $HO_2CH_2CO=>CH_2O+CO+OH$. The under-prediction of CO does not, however, influence the good prediction of CO_2, which is produced at LT by the β-scission of CH_3CO_2 that is an important radical of DEE primary mechanism and produced *via* the formation of the ketohydroperoxide HOOQ1=O (compare also Fig. 6 in the main paper). Under PFR conditions, simultaneous inclusion of the tested uncertainty sources (temperature, pressure, rate coefficients of $DEE+C_xH_yO_2$ as detailed in the main paper) significantly enhances DEE conversion in the second NTC zones, improving the model-experiment agreement for major species in this zone. Note that the tested uncertainties do not significantly affect these species in other temperature windows.

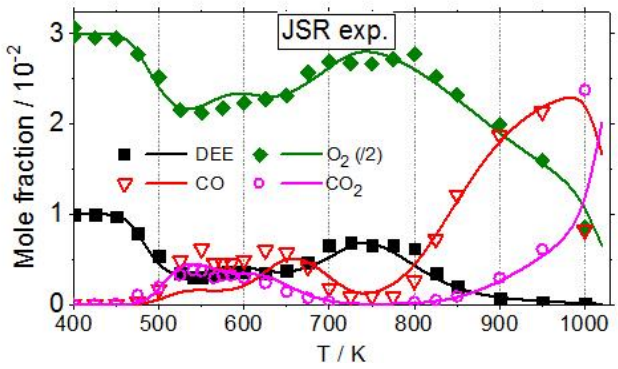

Fig. S8. JSR mole fraction profiles of major species (DEE, O_2, CO, CO_2). *Symbols:* experiment, *lines:* present model.

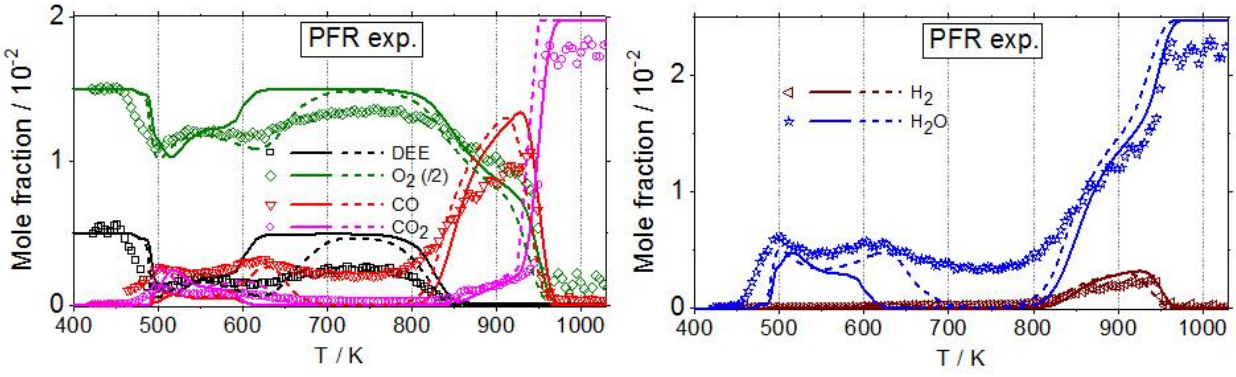

Fig. S9. PFR mole fraction profiles of major species (DEE, O_2, CO, CO_2, H_2, H_2O). Symbols: experiment, *solid lines*: simulations with the present model, and *dashed-lines*: simulations with the present model including simultaneously the tested uncertainties as detailed in the main paper.

Peak mole fraction of intermediate species from JSR and PFR

Table S2 presents peak mole fractions of intermediates measured for DEE oxidation (ϕ=1) in the JSR and PFR experiment, together with predictions by the present model.

Table S2: Intermediate species detected in DEE oxidation (ϕ=1) with predictions by the present model. **M**: nominal mass. $\mathbf{x_{max}}$: peak mole fraction. **T**: temperature at x_{max} (K). [a] including methanol because the used GC system could not separate it from acetaldehyde. [b] 2-methyl-1,3-dioxolane. [c] peak tailing, ambiguous peak location. [d] failed predictions in ~600-800 K due to no simulated fuel's reactivity. [e] same mass of fuel. [f] unavailable EI cross section. ***Italic-bold*** font highlights intermediates containing 2-3 O-atoms with peak mole fraction found at relatively low temperature.

M	Species		JSR				PFR			
			Experiment		Simulation		Experiment		Simulation	
			x_{max}	T	x_{max}	T	x_{max}	T	x_{max}	T
16	CH_4	Methane	2.0E-3	900	2.7E-3	880	1.5E-3	867	1.7E-3	870
28	C_2H_4	Ethylene	4.8E-3	850	5.3E-3	840	3.3E-3	867	3.7E-3	850
30	C_2H_6	Ethane	2.3E-4	850	1.6E-4	880	9.8E-5	837	1.7E-4	860
	CH_2O	Formaldehyde	1.9E-3	600	1.8E-3	670	1.5E-3	626	[d]	[d]
42	C_3H_6	Propene	5.2E-5	850	5.7E-5	830	2.3E-5	842	3.2E-5	860
44	CH_3CHO	Acetaldehyde	6.1E-3[a]	650	6.7E-3[a]	630	1.9E-3	700	[d]	[d]
	C_2H_4O-cy	Ethylene oxide	9.7E-5	850	2.1E-4	840			9.9E-5	860
46	C_2H_5OH	Ethanol	2.0E-5	600[c]	2.4E-5	540	1.4E-5	482[c]	4.4E-5	530
60	***CH_3COOH***	***Acetic acid***	***2.8E-3***	***525***	***2.7E-3***	***530***	***2.0E-3***	***502***	***1.5E-3***	***520***
	CH_3OCHO	***Methyl formate***	***1.1E-5***	***525***	***2.4E-7***	***650***			[d]	[d]
72	C_4H_8O, EVE	Ethyl vinyl ether	2.1E-5	700	7.2E-6	600	2.4E-5	700	[d]	[d]
74	***$C_3H_6O_2$, EF***	***Ethyl formate***	***1.2E-4***	***500***	***2.4E-4***	***510***	[e]	[e]	***1.9E-4***	***510***
88	***$C_4H_8O_2$, EA***	***Ethyl acetate***	***2.8E-5***	***525***	***4.6E-5***	***500***	[f]	***478***	***5.7E-5***	***520***
	$C_4H_8O_2$-cy	Me-dioxolane[b]	1.8E-4	625	1.6E-4	680			[d]	[d]
102	***$C_4H_6O_3$, AA***	***Acetic anhydride***	***1.7E-4***	***500***	***2.4E-4***	***510***	[f]	***482***	***9.5E-5***	***510***

Additional profiles of intermediate species from the PFR

While the mole fraction profiles of selected intermediates containing 0-1 O-atom from the JSR are presented in the main paper, Fig. S10 displays those obtained with the PFR. Some features of the behavior from the PFR seem to be similar in comparison to the JSR. Exemplarily, profiles of CH_4, C_2H_4, C_2H_6 and C_3H_6 reach their maximum at high temperatures above 800 K; the EVE profile peaks at around 700 K; while C_2H_5OH was detected at very low temperature; CH_2O and CH_3CHO are measured in high amounts over a large range of temperatures; CH_2O shows two peaks in the two highest LT fuel conversion zones. However, an important difference between the PFR and the JSR is the profile shape of several intermediates below 800 K. While several intermediates from the PFR show still certain quantities in the temperature range of 625-800 K, the present model cannot reproduce the formation of these species in this temperature range, unfortunately, because the model failed to predict DEE conversion (compare Fig. S9 above and Fig. 2b of the main paper). Including some uncertainty sources (temperature, pressure, rate coefficients of DEE+$C_xH_yO_2$) in the simulations improves the model-experiment agreement as discussed above and in the main paper, but discrepancies remain within the range of 700-800 K. Note that with the current model analyses, the DEE chemistry in both reactors is very similar, *i.e.* sensitivity analyses presented in Fig. S5 above is

applicable for both reactors. As a consequence, further modifications of the rate coefficients of the currently-considered reaction classes which would increase the system reactivity in the PFR will also affect the quality of the simulations under JSR conditions. Therefore, identification of possible new reaction classes that are sensitive for PFR but not for JSR conditions as well as consideration of possible two-dimensional effects in PFR simulations may improve the current quality of prediction.

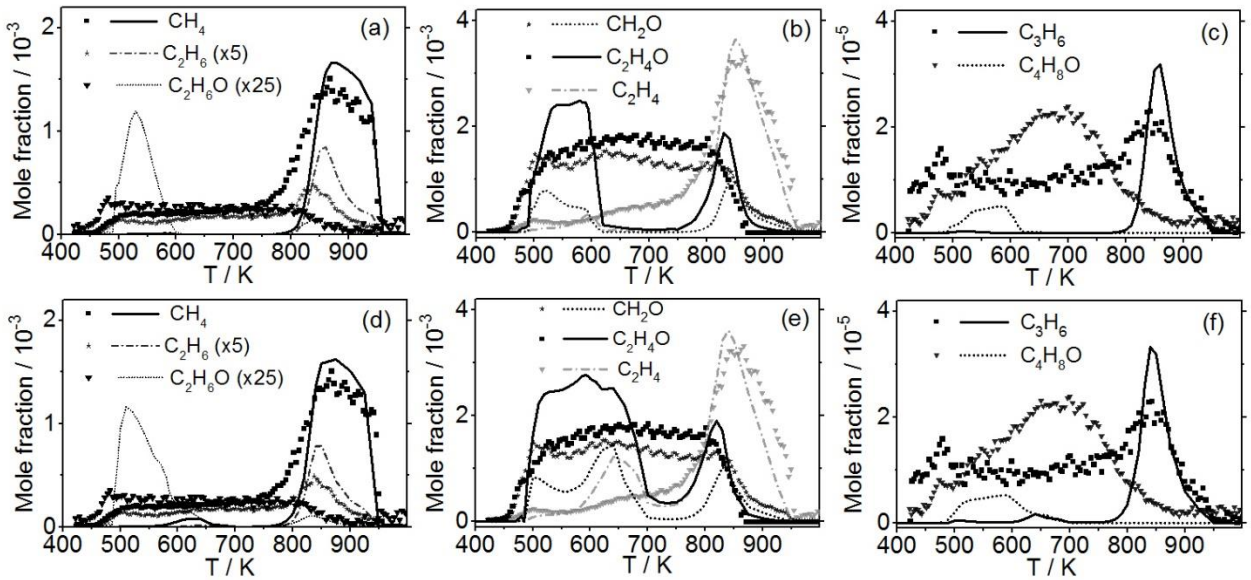

Fig. S10. PFR mole fraction profiles of selected intermediates containing 0-1 O-atom. *Symbols:* experiment; *lines:* model. Simulation results for *(a-c)* were obtained with the present model, and for *(d-f)* with the present model considering simultaneously the tested uncertainties as discussed in the main paper.

References

[S1] Y. Sakai, J. Herzler, M. Werler, C. Schulz, M. Fikri, Proc. Combust. Inst. 36 (2017) 195-202.

[S2] S. Thion, C. Togbé, Z. Serinyel, G. Dayma, P. Dagaut, Combust. Flame 185 (2017) 4-15.

[S3] J. Bugler, A. Rodriguez, O. Herbinet, F. Battin-Leclerc, C. Togbé, G. Dayma, P. Dagaut, H. J. Curran. Proc. Combust. Inst. 36 (2017) 441-448.

[S4] Y. Sakai, H. Ando, H. K. Chakravarty, H. Pitsch, R. X. Fernandes, Proc. Combust. Inst. 35 (2015) 161-169.

[S5] J. Eble, J. Kiecherer, M. Olzmann, Z. Phys. Chem. 231 (10) (2017) 1603-1623.

[S6] A. Jalan, I.M. Alecu, R. Meana-Pañeda, J. Aguilera-Iparraguirre, K.R. Yang, S.S. Merchant, D.G. Truhlar, W.H. Green, J. Am. Chem. Soc. 135 (30) (2013) 11100-11114.

[S7] Z. Wang, X. Zhang, L. Xing, L. Zhang, F. Herrmann, K. Moshammer, F. Qi, K. Kohse-Höinghaus, Combust. Flame 162 (4) (2015) 1113-1125.

[S8] C.W. Gao, J.W. Allen, W.H. Green, R.H. West, Comput. Phys. Commun. 203 (2016) 212-225.

[S9] E. Hu, Y. Chen, Z. Zhang, J.-Y. Chen, Z. Huang, Fuel 209 (2017) 509-520.

[S10] S.A. Carr, D.R. Glowacki, C.-H. Liang, M.T. Baeza-Romero, M.A. Blitz, M.J. Pilling, P.W. Seakins. J. Phys. Chem. A 115 (6) (2011) 1069-1085.

[S11] W. Sun, T. Tao, R. Zhang, H. Liao, C. Huang, F. Zhang, X. Zhang, Y. Zhang, B. Yang, Combust. Flame 185 (2017) 173-187.

[S12] K. Yasunaga, F. Gillespie, J.M. Simmie, H.J. Curran, Y. Kuraguchi, H. Hoshikawa, M. Yamane, Y. Hidaka, J. Phys. Chem. A 114 (34) (2010) 9098-9109.

[S13] M. Werler, L.R. Cancino, R. Schiessl, U. Maas, C. Schulz, M. Fikri, Proc. Combust. Inst. 35 (2015) 259-266.

[S14] N. Vin, O. Herbinet, F. Battin-Leclerc, J. Anal. Appl. Pyrolysis 121 (2016) 173-176.

[S15] L.-S. Tran, J. Pieper, H.-H. Carstensen, H. Zhao, I. Graf, Y. Ju, F. Qi, K. Kohse-Höinghaus, Proc. Combust. Inst. 36 (2017) 1165-1173.

[S16] U. Burke , K.P. Somers, P. O'Toole, C.M. Zinner, N. Marquet, G. Bourque, E.L. Petersen, W.K. Metcalfe, Z. Serinyel, H.J. Curran, Combust. Flame 162 (2015) 315-330.